A Conserved Tryptophan in Nitric Oxide Synthase Regulates Heme−Dioxy Reduction by Tetrahydrobiopterin[†]

Zhi-Qiang Wang,[‡] Chin-Chuan Wei,[‡] Sanjay Ghosh,[‡,§] Abigail L. Meade,[‡] Craig Hemann,[||] Russ Hille,[||] and Dennis J. Stuehr*[,‡]

Department of Immunology, The Lerner Research Institute, Cleveland Clinic Foundation, Cleveland, Ohio 44195, and Department of Molecular and Cellular Biochemistry, The Ohio State University, Columbus, Ohio 43210

Received June 8, 2001; Revised Manuscript Received August 9, 2001

ABSTRACT: In nitric oxide synthase (NOS), (6*R*)-tetrahydrobiopterin (H_4B) binds near the heme and can reduce a heme−dioxygen intermediate ($Fe^{II}O_2$) during Arg hydroxylation [Wei, C.-C., Wang, Z.-Q., Wang, Q., Meade, A. L., Hemann, C., Hille, R., and Stuehr, D. J. (2001) *J. Biol. Chem. 276*, 315−319]. A conserved Trp engages in aromatic stacking with H_4B, and its mutation inhibits NO synthesis. To examine how this W457 impacts H_4B redox function, we performed single turnover reactions with the mouse inducible NOS oxygenase domain (iNOSoxy) mutants W457F and W457A. Ferrous mutants containing Arg and H_4B were mixed with O_2-containing buffer, and then heme spectral transitions, H_4B radical formation, and Arg hydroxylation were followed versus time. A heme $Fe^{II}O_2$ intermediate was observed in W457A and W457F and had normal spectral characteristics. However, its disappearance rate (6.5 s^{-1} in W457F and 3.0 s^{-1} in W457A) was slower than in wild-type (12.5 s^{-1}). Rates of H_4B radical formation (7.1 s^{-1} in W457F and 2.7 s^{-1} in W457A) matched their rates of $Fe^{II}O_2$ disappearance, but were slower than radical formation in wild-type (13 s^{-1}). The extent of H_4B radical formation in the mutants was similar to wild-type, but their radical decayed 2−4 times faster. These kinetic changes correlated with slower and less extensive Arg hydroxylation by the mutants (wild-type > W457F > W457A). We conclude that W457 ensures a correct tempo of electron transfer from H_4B to heme $Fe^{II}O_2$, possibly by stabilizing the H_4B radical. Proper control of these parameters may help maximize Arg hydroxylation and minimize uncoupled O_2 activation at the heme.

Nitric oxide synthases (NOS)[1] are homodimeric enzymes whose subunits contain an N-terminal oxygenase and a C-terminal reductase domain (*1*−*4*). The NOS oxygenase domain binds Fe-protoporphyrin IX (heme), Arg, and the essential cofactor (6*R*)-tetrahydrobiopterin (H_4B). Two oxygenase domains associate to form the dimer interface, thus creating two active sites per homodimer. Attached reductase domains bind FAD, FMN, and NADPH and support catalysis by providing electrons to the oxygenase domains.

Because NOS are the only enzymes known to contain both heme and H_4B, how these groups participate in NO synthesis is a topic of interest. NO synthesis occurs in two steps: Arg is first hydroxylated to form N^{ω}-hydroxyarginine (NOHA) as an enzyme-bound intermediate, and then NOHA is oxidized to NO plus citrulline (*1*−*4*). Each step represents a mixed-function oxidation that consumes a molecule of O_2 and utilizes NADPH-derived reducing equivalents. Crystal structures of NOS oxygenase domain dimers (NOSoxy) (*5*−*8*) show that Arg and NOHA are held directly above the heme, consistent with the heme binding O_2 and activating it for substrate oxidation. Indeed, ferrous NOS binds O_2 to form a detectable but transient ferrous−dioxy intermediate ($Fe^{II}O_2$) (*9*−*11*). During NO synthesis, a second electron must be provided to the $Fe^{II}O_2$ intermediate to form the ultimate oxidant(s) that react(s) with Arg or NOHA. H_4B binds near the heme in such a way that it could provide an electron to the heme (Figure 1). Observations that bound H_4B becomes oxidized during limited catalysis (*12*, *13*) and forms a radical when O_2 reacts with ferrous NOSoxy proteins (*14*−*16*) support a redox role for H_4B.

We recently combined stopped-flow, rapid-quench, and rapid-freeze techniques to investigate the temporal and quantitative relationships among heme transitions, H_4B radical formation, and Arg hydroxylation during a single catalytic turnover by mouse inducible NOSoxy (iNOSoxy) (*15*). Our work revealed the following: (i) H_4B radical formation starts after an $Fe^{II}O_2$ intermediate forms; (ii) the rate of H_4B radical formation matches the rates of $Fe^{II}O_2$ disappearance and Arg hydroxylation. These data suggest a mechanism whereby H_4B transfers an electron to the $Fe^{II}O_2$

[†] This work was supported by National Institutes of Health Grants GM51491 and CA53914 (to D.J.S.) and GM58481 (to R.H.).

* Correspondence should be addressed to this author at the Department of Immunology NB-3, The Lerner Research Institute, Cleveland Clinic Foundation, 9500 Euclid Ave., Cleveland, OH 44195. Phone: 1-216-445-6950. FAX: 1-216-444-9329. E-mail: stuehrd@ccf.org.

[‡] The Lerner Research Institute.

[§] Present address: Department of Biochemistry, University College of Sciences, Calcutta 700 019, India.

[||] The Ohio State University.

[1] Abbreviations: NOS, nitric oxide synthase; Arg, L-arginine; DTT, dithiothreitol; NO, nitric oxide; HEPES, *N*-(2-hydroxyethyl)piperazine-*N*′-2-ethanesulfonic acid; NOHA, N^{ω}-hydroxy-L-arginine; HPLC, high-performance liquid chromatography; EPR, electron paramagnetic resonance; H_4B, (6*R*)-5,6,7,8-tetrahydro-L-biopterin; H_2B, 7,8-dihydro-L-biopterin; iNOSoxy, the oxygenase domain of inducible nitric oxide synthase.

10.1021/bi011182s CCC: $20.00
Published on Web 10/03/2001

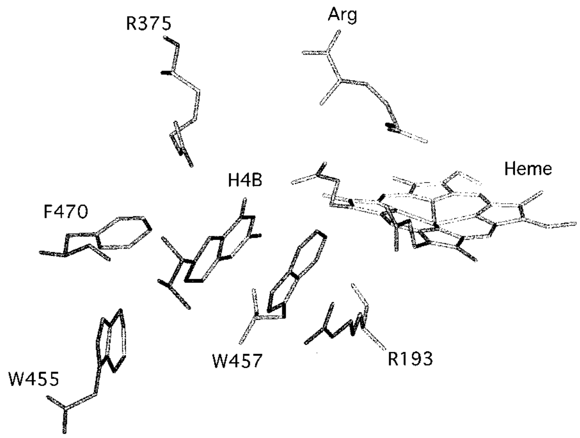

FIGURE 1: Residues whose side chains interact with the ring of H_4B. W455 and F470 residues are contributed by the partner subunit. Bound Arg and heme are indicated. Based on the crystal structure of the mouse iNOSoxy dimer 1NOD (5).

intermediate to create the ultimate oxidant, which then can quickly hydroxylate Arg. Because reduction of $Fe^{II}O_2$ by H_4B appears to be faster than heme reduction by NOS reductase domains (*17*, *18*), we have proposed that H_4B may be a kinetically preferred source of the second electron that helps NOS couple its O_2 reduction to Arg hydroxylation and NO synthesis (*19*).

Given the temporal and quantitative links between H_4B radical formation, $Fe^{II}O_2$ reduction, and Arg hydroxylation in wild-type iNOSoxy, we wished to examine how protein structure impacts these processes. Electron transfer between H_4B and the $Fe^{II}O_2$ intermediate is likely influenced by their structural proximity and by the surrounding amino acid residues. In mouse iNOS, the H_4B ring interacts with a number of highly conserved residues (Figure 1). Two residues (W457, R375) are provided by the same subunit while another two (F470, W455) are provided by the partner subunit of the dimer. All of these residues contact H_4B through π-stacking and/or hydrogen-bonding interactions (Figure 1, also see refs *5*, *8*, *20*). The importance of each residue regarding subunit dimerization and NO synthesis was recently investigated in iNOSoxy and neuronal NOS through site-directed mutagenesis studies (*21*, *22*). In particular, mutation of W457 to Ala and Phe in iNOSoxy allowed for dimerization but diminished NO synthesis by iNOS heterodimers containing the mutant subunits (wild-type > W457F > W457A) (*21*). To better understand how W457 controls H_4B and NOS catalytic functions, we have examined how W457A and W457F mutations impact heme transitions, H_4B radical formation, and Arg hydroxylation during a single turnover reaction by iNOSoxy. An accompanying paper by Aoyagi et al. (*20*) reports on the crystal structures of these two iNOSoxy mutants. Together our studies help define how H_4B participates in O_2 activation and how its redox functions are modulated by the surrounding protein structure.

MATERIALS AND METHODS

Materials and Enzyme Preparation. All reagents were obtained from Sigma or from sources reported previously (*15*). NOHA was a kind gift from Dr. Bruce King, Wake Forest University. Wild-type and mutant iNOSoxy proteins (amino acids 1−498 plus a 6-his extension at the C-terminus) were overexpressed in BL21 using the pCWori vector and purified as reported previously (*21*). Concentrations of iNOSoxy are given on a per heme basis (one heme incorporated per monomer), as determined by absorbance difference measurement at 444−500 nm for the ferrous−CO complex, using an extinction coefficient of 76 mM^{-1} cm^{-1}.

Enzyme Solution Preparation. W457 mutants were preincubated with Arg plus H_4B or H_2B on ice overnight before performing experiments, because of their lower affinity toward substrate and cofactor (*21*). Ferrous iNOSoxy proteins were generated as described previously (*15*). Briefly, overnight-incubated ferric proteins were placed in a cuvette, and graded amounts of a dithionite solution were added under anaerobic conditions, monitoring heme reduction spectroscopically. Full heme reduction typically required adding a slight molar excess of dithionite. All single turnover experiments were repeated at least 3 times using different batches of iNOSoxy proteins.

Stopped-Flow Spectroscopy. Rapid scanning measurements were carried out in a Hi-Tech (SF-61) stopped-flow apparatus equipped for anaerobic work and coupled to a Hi-Tech diode array detector. Ferric iNOSoxy proteins were diluted in N_2-purged Hepes buffer (50 mM, pH 7.5) containing DTT, H_4B or H_2B, and Arg. After reduction by dithionite, solutions were transferred into the stopped-flow instrument using a gastight syringe. Reactions mixed equal volumes of anaerobic enzyme solutions with air-saturated Hepes buffer at 10 °C. Final (post mixing) concentrations for wild-type iNOSoxy were 10 μM protein, 100 μM H_4B or H_2B, 0.5 mM DTT, and 100 μM Arg. Final concentrations for the W457 mutants were 5−10 μM protein, 1 mM H_4B or H_2B, 3 mM DTT, and 1 mM Arg. Ninety-six spectral scans were obtained after each mixing. Sequential spectral data were fit to different reaction models using the Specfit global analysis program (provided by Hi-Tech Ltd.), which could calculate the number of different enzyme species, their spectra, and their concentrations versus time during the single turnover reactions. In some cases, reacted samples were collected from the exit loop of the instrument and frozen immediately in dry ice for product analysis by HPLC.

Rapid-Quench Experiments. The kinetics of Arg oxidation during the single turnover reaction were studied using a Hi-Tech rapid-quench instrument and [^{14}C]Arg as described previously for wild-type iNOSoxy (*15*). In general, solutions of reduced ferrous iNOSoxy proteins containing H_4B and Arg were rapidly mixed with an equal volume of air-saturated buffer containing 10 mM Arg at 10 °C followed by rapid quenching with the same volume of acidic 2-propanol. Analysis of amino acids present in the quench flow reactions is described elsewhere (*15*). We used relatively high concentrations of mutant iNOSoxy proteins and [^{14}C]Arg due to their lower binding affinity toward Arg (*21*). Reactions contained 3 μM wild-type or W457A protein plus 2 μM [^{14}C]-Arg, and 20 μM W457F protein plus 10 μM [^{14}C]Arg. Otherwise, ferrous protein solutions were prepared as described above for the rapid scanning experiments.

Rapid-Freeze EPR Experiments. Experimental conditions for rapid-freeze reactions and EPR spectroscopy were as previously reported (*15*). The initial concentrations of mutant proteins, H_4B, and Arg were ∼270 μM, 1 mM, and 10 mM, respectively, and the reactions were done at 10 °C.

EPR Data Analysis. To estimate how much bound H_4B formed a radical during the single turnover reactions, the H_4B radical concentration determined at each time point was fit to a kinetic model as follows:

$$A \xrightarrow[k_1]{} B \xrightarrow[k_2]{} C$$

where A, B, and C are H_4B, its radical, and the oxidized radical (diamagnetic), respectively, and k_1 and k_2 are rate constants for radical formation and decay. The equation developed from this kinetic model was

$$[B] = [B_T]\left[\frac{k_1}{-k_1 + k_2}\right][e^{(-k_1(t+dt))} - e^{(-k_2(t+dt))}]$$

[B] is the concentration of H_4B radical present at each time point. $[B_T]$ is the total concentration of H_4B that formed a radical during the reaction, and dt is the lag time of radical formation. Values for $[B_T]$, k_1, k_2, and dt were determined by curve-fitting using the above equation and Delta Graph software (*15*). The percentage of H_4B that formed a radical in each iNOSoxy protein was calculated as $[B_T]/[\text{iNOSox}]_{total} \times 100$. We assumed all iNOSoxy heme proteins contained one H_4B bound per heme.

Product Stoichiometry Analyses. NOHA production from Arg was measured by two different methods. (i) Reaction samples collected from single turnover reactions run in anaerobic vessels or collected from stopped-flow rapid scanning experiments (see above) were derivatized with *o*-phthalaldehyde, and then analyzed by reverse-phase HPLC with fluorescence detection as described previously (*10*, *23*). Reactions contained 1, 2, or 5 mM Arg. After reactions were completed, sample solutions were filtered through an Amicon Centricon device (10 000 MW cutoff) prior to derivatization for 2 min. An aliquot was then immediately injected into a Hewlett-Packard ODS-Hypersil column and eluted with a gradient of buffer A (5 mM ammonium acetate, pH 6.0, 20% methanol) and buffer B (100% methanol). Retention times and concentrations of amino acids were calculated based on Arg and NOHA standard solutions. (ii) NOHA formation was measured by rapid-quench experiments using $[^{14}C]$Arg. For W457A, 10 μM protein was incubated with 10 μM $[^{14}C]$-Arg, 140 μM Arg, and 1 mM H_4B prior to reaction. For W457F, 20 μM protein was incubated with 20 μM $[^{14}C]$-Arg, 80 μM Arg, and 1 mM H_4B. Because these conditions should allow only ~50% Arg binding to W457F iNOSoxy as judged from published binding data (*21*), we assumed 50% binding saturation when calculating W457F product stoichiometry by this method.

RESULTS

All single turnover reactions were done at 10 °C and were initiated by rapid mixing an oxygen-containing buffer with a prereduced ferrous iNOSoxy protein that contained H_4B (or H_2B) and Arg. The reaction mixture then underwent rapid UV−visible scanning to follow heme transitions, or was aged for various times followed by rapid freezing for EPR detection of the H_4B radical, or rapid chemical quenching to follow Arg conversion to products.

Spectral Species and Heme Transitions. In wild-type iNOSoxy, one can discern three spectral species during the single turnover reaction. They are in order of appearance the initial ferrous iNOSoxy, an $Fe^{II}O_2$ intermediate, and ending ferric enzyme (*15*). In reactions using the W457A and W457F iNOSoxy mutants, we discerned these same three spectral species. Figure 2 contains recorded spectra (left panels) and calculated spectra (right panels) from both W457 mutants undergoing single turnover reactions. Spectral traces and absorbance maxima for the ferrous, $Fe^{II}O_2$, and ferric species in both mutants were very similar to one another and to wild-type iNOSoxy (Table 1). There also was good agreement between the recorded and calculated spectra of the $Fe^{II}O_2$ or ferric species (Figure 2, Table 1). The Soret absorbance position of the mutant ferric proteins indicated that their heme groups were in a predominantly high spin state at the end of the single turnover reactions (Figure 2, Table 1). We conclude that the W457 mutations still permitted buildup of an $Fe^{II}O_2$ intermediate, and did not significantly alter its spectral characteristics or those of the ferrous or ferric species.

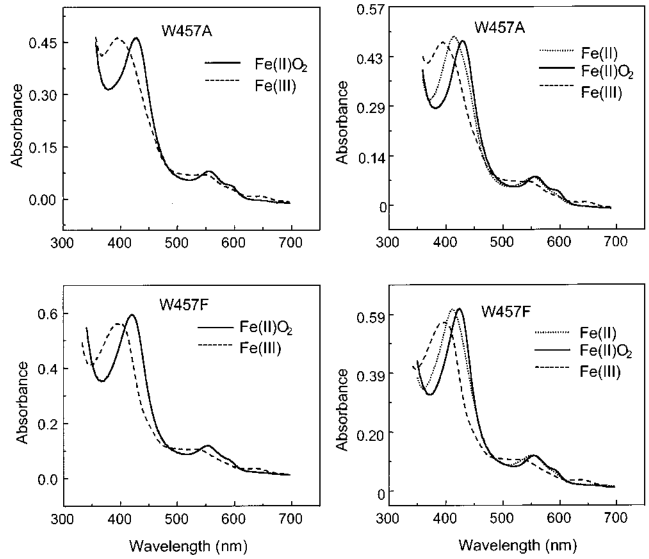

FIGURE 2: Light absorbance spectra of W457 mutants during Arg hydroxylation. Single turnover reactions contained 1 mM Arg and 1 mM H_4B, and were initiated by mixing anaerobic ferrous proteins with air-saturated buffer. See Materials and Methods for details. Left panels contain spectral scans collected at 0.061 s (—) and 0.66 s (- - -) after mixing, and highlight the $Fe^{II}O_2$ intermediate and ferric iNOSoxy species, respectively, for both mutants. Right panels contain spectra of the ferrous, $Fe^{II}O_2$, and ferric species as calculated from Specfit global analysis of the kinetic data. Data are representative of 3 or 4 independent experiments.

Table 1: Light Absorbance Data for Ferrous, $Fe^{II}O_2$, and Ferric Forms of Wild-Type, W457A, and W457F iNOSoxy[a]

	absorbance peak positions (nm)		
protein	ferrous	$Fe^{II}O_2$	ferric
wild-type	414 (412)	426 (426)	393 (396)
	553 (553)	553 (555)	643 (647)
		594 (593)	540 (541)
W457A	416 (413)	430 (428)	396 (396)
	554 (553)	556 (556)	644 (644)
		593 (594)	547 (547)
W457F	413 (414)	426 (422)	396 (398)
	555 (554)	555 (553)	638 (636)
		590 (586)	537 (536)

[a] Values were determined by Specfit analysis except for those in parentheses which were taken from selected kinetic traces.

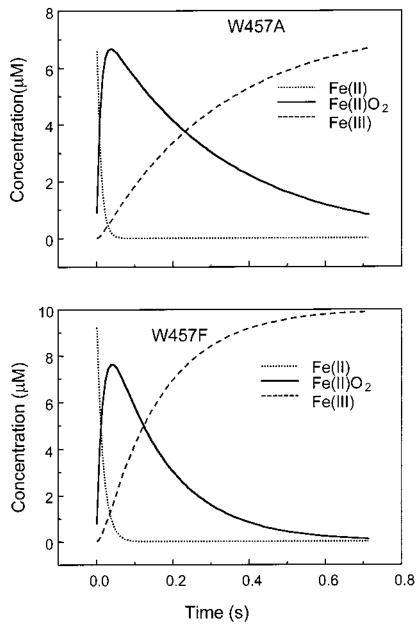

FIGURE 3: Concentration of ferrous, $Fe^{II}O_2$, and ferric species versus time during Arg hydroxylation by the W457 mutants. Based on Specfit global analysis of kinetic data from reactions described in Figure 2.

Table 2: Data from Arg Single Turnover Reactions for Wild-Type iNOSoxy and W457 Mutants[a]

	wild-type	W457F	W457A
$Fe^{II}O_2$ disappearance rate (s^{-1})[b]	12.5 ± 0.2	6.5 ± 0.1	3.0 ± 0.1
$Fe^{II}O_2$ disappearance rate + H_2B (s^{-1})[b]	0.30 ± 0.08	0.37 ± 0.01	0.052 ± 0.003
H_4B radical formation rate (s^{-1})[c]	13	7.1	2.7
H_4B radical decay rate (s^{-1})[c]	0.6	1.0	2.7
amount of H_4B radical formed per heme (%)[d]	100	78	72
rate of NOHA formation (s^{-1})[e]	9.2 ± 1.1	4.3 ± 1.2	2.6 ± 0.7
NOHA produced per heme	0.55 ± 0.06[f]	0.22 ± 0.13[f]	0.15 ± 0.06[f]
	0.43 ± 0.10[g]	0.30 ± 0.05[g] 0.32[h]	0.16 ± 0.06[g] 0.18[h]

[a] All reactions contained H_4B unless otherwise specified. [b] From two separate experiments of eight mixings ($n = 16$). [c] Rates calculated from two separate data sets containing 7−10 points each. [d] Calculated as explained under Materials and Methods. [e] Rates calculated from three separate data sets containing 5−8 points each. [f] Values obtained from reactions that contained [^{14}C]Arg ($n = 3$). [g] Values obtained from reactions that contained Arg at a concentration of 1 mM ($n = 6$). [h] Values obtained from reactions that contained Arg at a concentration of 5 mM ($n = 1$).

The two panels of Figure 3 show how concentrations of ferrous, $Fe^{II}O_2$, and ferric species change during a single turnover reaction for each mutant. Loss of the initial ferrous species, buildup of the $Fe^{II}O_2$ intermediate, and its conversion to ferric enzyme were best described by monophasic transitions in both mutants, as is the case for wild-type NOSoxy proteins (*9*, *10*, *15*). Observed rates of $Fe^{II}O_2$ formation ranged between 50 and 100 s^{-1} depending on the experiment and were relatively fast compared to $Fe^{II}O_2$ decay in both mutant and wild-type proteins. This allowed significant buildup of the $Fe^{II}O_2$ intermediate in all cases (Figure 3). Importantly, $Fe^{II}O_2$ disappearance in the W457F mutant was 1.9 times slower than wild-type iNOSoxy and in the W457A mutant was 4.2 times slower (Table 2). To help understand how bound H_4B influenced the kinetics of $Fe^{II}O_2$ disappearance, we repeated the reactions using H_2B-bound mutant and wild-type iNOSoxy proteins. In all cases, three species were observed whose spectral features were identical to the ferrous, $Fe^{II}O_2$, and ferric species in the H_4B-bound proteins (data not shown). However, conversion of the $Fe^{II}O_2$ intermediate to ferric enzyme was 20−60 times slower in the H_2B-saturated proteins, with W457A being the slowest (Table 2).

H_4B Radical Formation and Decay. Rapid-freeze experiments showed that a radical with *g* value 2.0 built up in W457A and W457F iNOSoxy during the single turnover reactions (Figure 4, left panel). The spectra and saturation properties of the mutant radicals were identical to those of the H_4B radical formed in wild-type iNOSoxy (Figure 4) (*14*, *15*). Signal intensities were used to calculate the amount of H_4B radical per heme that was present at each time point. Values for the two mutants and wild-type iNOSoxy are plotted versus time in the right panel and inset of Figure 4. Less H_4B radical accumulated during the W457F and W457A reactions compared to wild-type iNOSoxy. Increasing the H_4B concentration in the reactions from 1 to 3 mM did not alter the results in any way (data not shown), suggesting that the observed differences were not due to incomplete H_4B binding. The kinetic data were fit to a two-step process of radical formation and decay (solid and dashed lines in right panel of Figure 4). This gave calculated rates of radical formation in W457A and W457F of 7.1 and 2.7 s^{-1}, respectively, which are slower than in wild-type (13 s^{-1}, Table 2). The calculated rates of radical decay in W457F and W457A were 1.0 and 2.7 s^{-1}, which were faster than wild-type (0.6 s^{-1}, Table 2). Our data analysis also estimated that 72%, 78%, and 100% of bound H_4B formed a radical (per heme) during the single turnover reactions of W457A, W457F, and wild-type iNOSoxy, respectively (Table 2).

Arg Hydroxylation. We next studied the stoichiometry and kinetics of Arg hydroxylation in the W457 mutants. For stoichiometry studies, some of the single turnover reactions contained different concentrations of Arg (1, 2, and 5 mM) to ensure that data were being obtained under saturation binding conditions. The W457F and W457A mutants consistently catalyzed one-half and one-third as much Arg hydroxylation as wild-type iNOSoxy on a per heme basis (Table 2). NOHA was the only amino acid product in all cases, and its formation depended completely on H_4B (data not shown).

Figure 5 shows the kinetics of [^{14}C]Arg disappearance and [^{14}C]NOHA formation in the single turnover reactions as determined by rapid-quench analysis. These experiments contained [^{14}C]Arg concentrations that were substoichiometric with respect to enzyme, and thus provide information on the rate but not the extent of Arg hydroxylation. The data fit well to a single exponential process in all cases. Rates of Arg disappearance and NOHA formation were equivalent within experimental error. They were 4.3 and 2.6 s^{-1} for W457F and W457A, respectively, which are slower than in wild-type iNOSoxy (9.2 s^{-1}, Table 2).

DISCUSSION

Our results build on mechanistic concepts advanced in previous studies (*14*−*17*, *19*) and provide new insight into

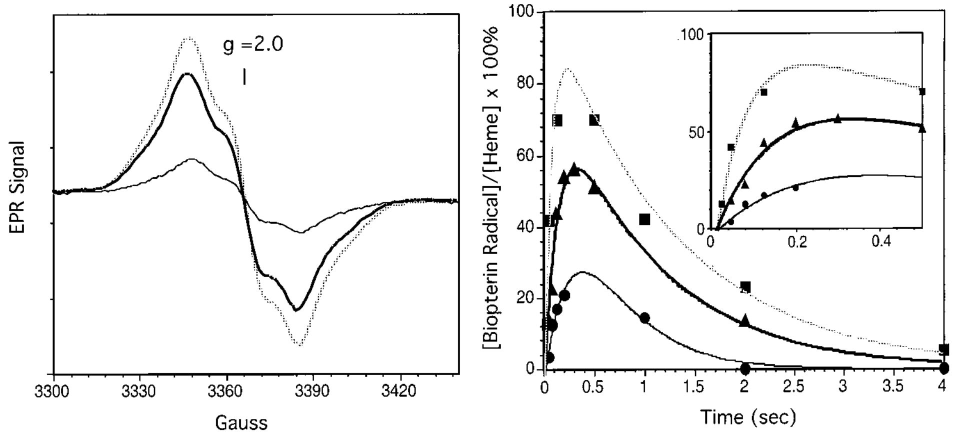

FIGURE 4: H_4B radical formation and decay during Arg hydroxylation in W457 mutants and wild-type iNOSoxy. Anaerobic ferrous iNOSoxy proteins containing 10 mM Arg and 1 mM H_4B were rapidly mixed with an O_2-saturated solution at 10 °C to start the reaction; reactions were aged for the indicated times, and then quenched by rapid freezing. Left panel: EPR traces were recorded at 125 ms for wild-type (dashed line), 300 ms for W457F (thick line), and 200 ms for W457A (thin line) after initiating the reaction. Right panel: Calculated concentrations of the H_4B radical versus time for wild-type (■), W457F (▲), or W457A (●) reactions. Curve fitting was done as described under Materials and Methods. Data are representative of two experiments.

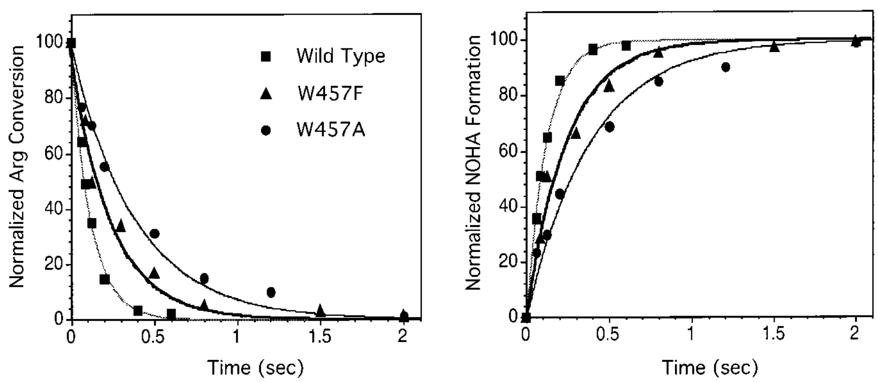

FIGURE 5: Arg disappearance and NOHA formation in W457 mutants and wild-type iNOSoxy during a single catalytic turnover. Anaerobic solutions of ferrous iNOSoxy proteins W457F (▲), W457A (●), and wild-type (■) that contained H_4B and substoichiometric quantities of [^{14}C]Arg were rapidly mixed with an air-saturated solution at 10 °C to start the reaction. Reactions were aged for the indicated times and then rapidly quenched with acidic 2-propanol. See Materials and Methods for details. The percentage [^{14}C]Arg conversion to [^{14}C]NOHA in each single turnover reaction was 39%, 28%, and 22% for wild-type, W457F, and W457A proteins, respectively. These values were used to normalize concentrations of [^{14}C]Arg or [^{14}C]NOHA among the three proteins to best compare their time courses. Data are representative of three experiments.

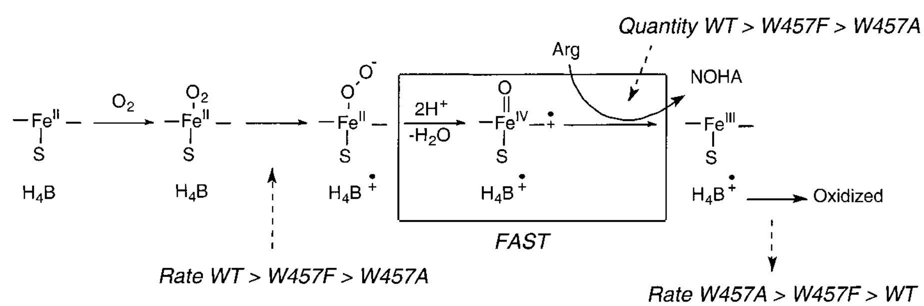

FIGURE 6: Effect of W457 mutations on various aspects of Arg hydroxylation by iNOSoxy. Both mutations altered the rates of H_4B radical formation and decay, and also diminished the amount of Arg hydroxylated in the single turnover reaction. Steps that occur after H_4B transfers an electron to $Fe^{II}O_2$ are fast relative to the electron transfer itself. Although the H_4B radical is shown as a cation, it could also be uncharged. See text for details.

NOS structure–function (Figure 6). Both W457 mutants maintained an ability to oxidize H_4B to its radical during the single turnover reaction. Because both mutants are partially active in NO synthesis assays (*21*), our current finding reinforces the connection between H_4B redox function and NO synthesis. It is also consistent with structural data showing that H_4B is bound in its normal position near the heme in both W457 mutants (see accompanying paper, ref *20*). As in wild-type iNOSoxy (*15*), the rate of H_4B radical formation in both mutants was closely coupled to disappearance of their $Fe^{II}O_2$ intermediate. This process was in turn kinetically coupled to their Arg hydroxylation (or NOHA formation) and to regeneration of ferric enzyme. Such strong kinetic correlates support the concept that H_4B radical formation represents electron transfer from H_4B to the $Fe^{II}O_2$ intermediate. Thus, W457 mutants appear to conserve the fundamental redox functions of their H_4B and heme groups, and proceed through a standard catalytic mechanism: Ferrous heme binds O_2 to generate the $Fe^{II}O_2$ intermediate, which then receives an electron from H_4B to generate a heme-based oxidant that can hydroxylate Arg. Because Arg hydroxylation by the W457 mutants was as fast as their H_4B radical formation and $Fe^{II}O_2$ disappearance within experimental error, we conclude that H_4B electron transfer remained rate-limiting for Arg hydroxylation by the mutant ferrous proteins.

W457 mutations clearly altered the rates of H_4B radical formation and decay in our single turnover reactions. However, they appeared to have little impact on the amount of H_4B that formed a radical. This conclusion is suggested by our calculation that the mutants generated 0.7−0.8 H_4B radical per heme during their reactions (Table 2), and by our observing single exponential rates of $Fe^{II}O_2$ disappearance in both mutants that were equivalent to their rates of H_4B radical formation. Thus, electron transfer between H_4B and the $Fe^{II}O_2$ intermediate appeared to be practically complete and well-coupled in both W457 mutants. This is also the case in wild-type iNOSoxy (*15*). If H_4B electron transfer were incomplete or poorly coupled in the W457 mutants, then we should have observed biphasic rates for their $Fe^{II}O_2$ disappearance, where the slow rate component matches rates obtained with H_2B-loaded mutant proteins (H_2B cannot reduce the $Fe^{II}O_2$ intermediate). Since $Fe^{II}O_2$ disappearance was 20−60 times slower in H_2B-loaded proteins compared to H_4B-loaded proteins (see Table 1), biphasic decay corresponding to incomplete or uncoupled electron transfer would have been easily detected during analysis of the kinetic spectral data. Therefore, we conclude that W457 primarily regulates the tempo of electron transfer between H_4B and the $Fe^{II}O_2$ intermediate, rather than influences the extent or coupling of the electron transfer. Its kinetic function may be important, because slowing down H_4B electron transfer by a factor of 2 in W457F or 4 in W457A was associated with the mutants catalyzing proportionally less Arg hydroxylation than wild-type iNOSoxy (Table 2, Figure 6).

W457A and W457F iNOSoxy mutants had diminished rates of NO synthesis in iNOS heterodimer studies (activity of wild-type ≥ W457F > W457A; see ref *21*). Also, NO synthesis activities of full-length W457A iNOS[2] and corresponding neuronal NOS mutants W678L and W678H (*22*) were less than wild-type, and were uncoupled with respect to enzyme NADPH oxidation. These catalytic profiles are consistent with our single turnover results. Specifically, W457 mutations primarily slowed the rate of H_4B radical formation and sped up radical decay. Slower electron transfer from H_4B to $Fe^{II}O_2$ could uncouple NOS oxygen activation from NO synthesis if $Fe^{II}O_2$ decay is sufficiently fast in full-length NOS, as may be the case (*17*). In such a circumstance, superoxide release from the $Fe^{II}O_2$ intermediate would occur at the expense of NADPH oxidation, and would uncouple NADPH oxidation from NO synthesis in NOS.

Faster decay of the H_4B radical could also diminish NO synthesis and uncouple NADPH consumption, but by a different mechanism. Because fully reduced H_4B is required in both steps of NO synthesis (*10*, *11*, *23*), the H_4B radical formed during Arg hydroxylation must be reduced back to H_4B before starting the second step of NO synthesis. Reduction of the H_4B radical must occur before it undergoes oxidative decay, because NOS cannot reduce further oxidized species such as H_2B (*24*). The NOS reductase domain is expected to reduce the H_4B radical. Although the rate is unknown, it must be faster than oxidative decay of the H_4B radical in wild-type NOS enzymes to keep their NADPH oxidation coupled to NO synthesis. Indeed, the available data show that H_4B radical decay is relatively slow in wild-type iNOSoxy (*14*, *15*, this report), but its decay in the W457 mutants is faster. In W457A iNOSoxy, the rate of H_4B radical decay (2.5 s^{-1}) approaches or exceeds the rate of heme reduction in full-length iNOS (1−2 s^{-1}) when determined under similar conditions (*18*, *25*). In principle, the W457 mutations might promote oxidation of the H_4B radical by increasing its exposure to solvent or by causing it to dissociate from the enzyme. Structural changes related to these possibilities are discussed in the accompanying paper (*20*). Although it will ultimately be important to compare rates of H_4B radical formation, reduction, and decay in full-length NOS enzymes, measuring these rates may be challenging because full-length NOS contain a stable flavin semiquinone radical (*26*−*29*) that complicates interpretation of the EPR data.

Wild-type NOSoxy proteins consistently generate substoichiometric amounts of NOHA from Arg in single turnover experiments (*10*−*12*, *14*, *15*, *23*). How the W457 mutations further diminish the extent of Arg hydroxylation remains an open question. Previous spectroscopic studies suggest that the mutants have lower affinities toward Arg (*21*), thus raising the possibility of incomplete Arg binding. However, spectral traces recorded after the single turnover reactions show that the W457 mutant ferric hemes are in a predominantly high-spin state (Figure 2), which is attainable only when Arg binds to the H_4B-bound proteins. Moreover, yields of NOHA in these reactions did not increase upon increasing the initial Arg concentration from 1 to 5 mM (Table 2). These data argue against incomplete Arg binding being responsible for the different product yields. Because the extent of Arg hydroxylation correlated so well with rates of H_4B radical formation (wild-type > W457F > W457A), the kinetics of H_4B electron transfer may be an important factor in determining product yield. The simplest explanation is that slowing reduction of $Fe^{II}O_2$ by H_4B increases the likelihood that $Fe^{II}O_2$ will decay before it can be reduced. In theory, circumstances that increase the rate of H_4B radical formation and extent of Arg hydroxylation are possible. We are investigating this with H_4B analogues that appear to reduce the $Fe^{II}O_2$ intermediate faster than H_4B in single turnover experiments.[3] As a third possibility, W457 mutations might diminish the reactivity of the heme-based oxidant toward Arg. Because this effect would occur after H_4B reduces the $Fe^{II}O_2$ intermediate, it is surprising that its impact would vary so closely with the rates of H_4B electron transfer. The W457A mutation may alter heme reactivity during H_2O_2-driven NOHA oxidation, because in this assay the activity of H_4B-bound W457A iNOSoxy was less than wild-type, whereas the W457F mutant had a normal rate (*21*). The

[2] Wang, Z.-Q., and Stuehr, D. J., unpublished results.

[3] Wei, C.-C., and Stuehr, D. J., unpublished results.

[4] Santolini, J., Wang, Z.-Q., and Stuehr, D. J., unpublished results.

heme-based oxidant that forms when ferric NOS reacts with H_2O_2 is thought to be similar or identical to the species that hydroxylates Arg during normal NOS catalysis (*19*, *30*). Our crystallographic analysis of W457 mutants (see accompanying paper, ref *20*) shows that their overall structures are mostly unchanged compared to wild-type, including the heme environment. However, there are some changes in hydrogen bonding patterns near the heme, as well as increased mobility in discreet areas of the protein, that could conceivably influence heme reactivity. But the effects must be subtle, because both mutants formed $Fe^{II}O_2$ intermediates with spectral properties indistinguishable from wild-type, and the heme midpoint potential in W457A iNOSoxy is similar to wild-type.[4] We are investigating these issues by characterizing other NOS mutants that may have altered H_4B electron transfer, and by using H_4B or substrate analogues that modulate electron-transfer rates in NOS.

ACKNOWLEDGMENT

We thank members of the Stuehr, Tainer, and Getzoff laboratories for constructive advice and critical reading of the manuscript.

REFERENCES

1. Hemmens, B., and Mayer, B. (1998) *Methods Mol. Biol. 100*, 1−32.
2. Stuehr, D. J., and Ghosh, S. (1999) *Handb. Exp. Pharmacol. 143*, 33−70.
3. Marletta, M. A., Hurshman, A. R., and Rusche, K. M. (1998) *Curr. Opin. Chem. Biol. 2*, 656−663.
4. Ortiz de Montellano, P. R., Nishida, C., Rodriguez-Crespo, I., and Gerber, N. C. (1990) *Drug Metab. Dispos. 26*, 1185−1189.
5. Crane, B. R., Arvai, A. S., Ghosh, D. K., Wu, C. Q., Getzoff, E. D., Stuehr, D. J., and Tainer, J. A. (1998) *Science 279*, 2121−2126.
6. Raman, C. S., Li, H. Y., Martasek, P., Kral, A., Masters, B. S. S., and Poulos, T. L. (1998) *Cell 95*, 939−950.
7. Fischmann, T. O., Hruza, A., DaNiu, X., Fossetta, J. D., Lunn, C. A., Dolphin, E., Prongay, A. J., Paul, R., Lundell, D. J., Narula, S. K., and Weber, P. C. (1999) *Nat. Struct. Biol. 6*, 233−242.
8. Crane, B. R., Arvai, A. S., Ghosh, S., Getzoff, E. D., Stuehr, D. J., and Tainer, J. A. (2000) *Biochemistry 39*, 4608−4621.
9. Abu-Soud, H. M., Gachhui, R., Raushel, F. M., and Stuehr, D. J. (1997) *J. Biol. Chem. 272*, 17349−17353.
10. Boggs, S., Huang, L. X., and Stuehr, D. J. (2000) *Biochemistry 39*, 2332−2339.
11. Bec, N., Gorren, A. C., Voelker, C., Mayer, B., and Lange, R. (1998) *J. Biol. Chem. 273*, 13502−13508.
12. Witteveen, C. F. B., Giovanelli, J., and Kaufman, S. (1999) *J. Biol. Chem. 274*, 29755−29762.
13. Reif, A., Frohlich, L. G., Kotsonis, P., Frey, A., Bommel, H. M., Wink, D. A., Pfleiderer, W., and Schmidt, H. H. H. W. (1999) *J. Biol. Chem. 274*, 24921−24929.
14. Hurshman, A. R., Krebs, C., Edmondson, D. E., Huynh, B. H., and Marletta, M. A. (1999) *Biochemistry 38*, 15689−15696.
15. Wei, C.-C., Wang, Z. Q., Wang, Q., Meade, A., Hemann, C., Hille, R., and Stuehr, D. J. (2001) *J. Biol. Chem. 276*, 315−319.
16. Bec, N., Gorren, A. C. F., Mayer, B., Schmidt, P. P., Kristoffer, K. A., and Lange, R. (2000) *J. Inorg. Biochem. 81*, 207−211.
17. Stuehr, D. J., Pou, S., and Rosen, G. M. (2001) *J. Biol. Chem. 276*, 14533−14536.
18. Abu-Soud, H. M., Ichimori, K., Presta, A., and Stuehr, D. J. (2000) *J. Biol. Chem. 275*, 17349−17357.
19. Adak, S., Wang, Q., and Stuehr, D. J. (2000) *J. Biol. Chem. 275*, 33554−33561.
20. Aoyagi, M., Arvai, A. S., Ghosh, S., Stuehr, D. J., Tainer, J. A., and Getzoff, E. D. (2001) *Biochemistry 40*, 12826−12832.
21. Ghosh, S., Wolan, D., Adak, S., Crane, B. R., Kwon, N. S., Tainer, J. A., Getzoff, E. D., and Stuehr, D. J. (1999) *J. Biol. Chem. 274*, 24100−24112.
22. Sagami, I., Sato, Y., Daff, S., and Shimizu, T. (2000) *J. Biol. Chem. 275*, 26150−26157.
23. Abu-Soud, H. M., Presta, A., Mayer, B., and Stuehr, D. J. (1997) *Biochemistry 36*, 10811−10816.
24. Witteveen, C. F. B., Giovanelli, J., and Kaufman, S. (1996) *J. Biol. Chem. 271*, 4143−4147.
25. Presta, A., Siddhanta, U., Wu, C. Q., Sennequier, N., Huang, L. X., Abu-Soud, H. M., Erzurum, S., and Stuehr, D. J. (1998) *Biochemistry 37*, 298−310.
26. Stuehr, D. J., and Ikeda-Saito, M. (1992) *J. Biol. Chem 267*, 20547−20550.
27. Roman, L. J., Martasek, P., Miller, R. T., Harris, D. E., de La Garza, M. A., Shea, T. M., Kim, J. J., and Masters, B. S. (2000) *J. Biol. Chem. 275*, 29225−29232.
28. Noble, M. A., Munro, A. W., Rivers, S. L., Robledo, L., Daff, S. N., Yellowlees, L. J., Shimizu, T., Sagami, I., Guillemette, J. G., and Chapman, S. K. (1999) *Biochemistry 38*, 16413−16418.
29. Matsuda, H., and Iyanagi, T. (1999) *Biochim. Biophys. Acta 1473*, 345−355.
30. Rusche, K. M., Spiering, M. M., and Marletta, M. A. (1998) *Biochemistry 37*, 15503−15512.

BI011182S